Journal of Engineering Mathematics **42:** 265–282, 2002.

Free jets spun from a prilling tower

S.P. DECENT, A.C. KING and I.M. WALLWORK
School of Mathematics and Statistics, The University of Birmingham, Edgbaston, Birmingham, B15 2TT, UK
e-mail: spd@for.mat.bham.ac.uk, A.C.King@bham.ac.uk

Received 28 September 2001; accepted in revised form 15 March 2002

Abstract. A mathematical model of the dynamics of an inviscid liquid jet, subjected to both gravity and surface tension, which emerges from rotating drum is derived and analysed using asymptotic and computational methods. The trajectory and linear stability of this jet is determined. By use of the stability results, the break up length of the jet is calculated. Such jets arise in the manufacture of pellets (for example, of fertilizer or magnesium) using the prilling process. Here the drum would contain many thousands of holes, and the molten liquid would be pumped into the rotating drum. After the jet has broken up into droplets, these droplets solidify to form pellets. The jets in this prilling process are curved in space by both gravity and surface tension.

Key words: gravity, jet, pellets, prilling, rotation, surface tension.

1. Introduction

This paper is motivated by an industrial problem concerning the manufacture of pellets in the prilling process. Here a sieve-like cylindrical drum rotates about its axis, while molten liquid is pumped into the top of the drum. Liquid jets emerge from the various holes on the curved surface of the drum, and the jets break up due to centrifugal and capillary instability. The droplets produced by break up fall, against a counter current of cool air, and solidify to form pellets. This prilling process is widely used in industry, including in the manufacture of fertilizer (urea) and magnesium pellets.

Here we examine a mathematical model for a single inviscid liquid jet emerging from a rotating drum, determining the trajectory and stability of the jet. The trajectory of the jet is curved by both the rotation of the drum and by gravity. There have been numerous previous papers on straight liquid jets. Rayleigh [1] and Weber [2] carried out early studies into the stability of straight jets. Keller *et al.* [3] significantly extended these works by introducing the concept of the spatial stability of jets. There have been many recent studies of the effects of nonlinearity on the break up mechanisms of a straight liquid jet, including [4–7]. Significant experimental papers include [8–11]. However, we do not attempt to review all research on straight liquid jets here but refer the reader to reviews and books [12–15]. There are fewer previous papers that examine jets or liquid sheets with a curved centre line. Keller and Weitz [16] examined a liquid sheet which is curved by gravity. Without surface tension the sheet follows a ballistic path, while surface tension was found to make the sheet fall more sharply. Keller and Geer [17] analysed a curved slender liquid sheet with both free and solid boundaries. Tuck [18] examined a jet falling under gravity, without surface tension, following a ballistic path.

Wallwork *et al.* [19] investigated a slender liquid jet subjected to both rotation and surface tension. Theirs is a good model for prilling only if the rotational forces are much larger than

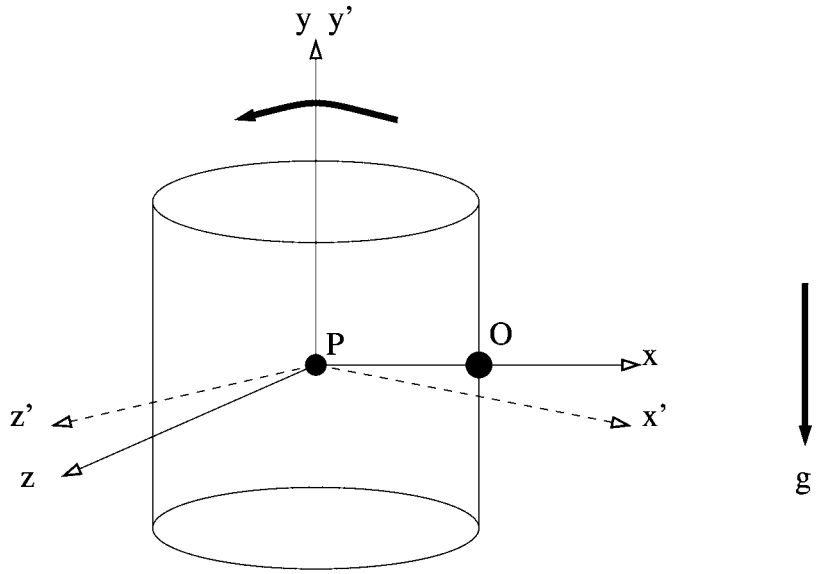

Figure 1. Sketch of the container, showing the fixed and rotating coordinate systems, and the directions of rotation and gravity.

those of gravity. This paper additionally incorporates gravity into this problem. This has the effect that the centreline of the jet no longer lies in a plane, but is taken off its plane by the action of gravity. In [19] a new coordinate system was introduced to facilitate the analysis of this type of system which is a curved variant of cylindrical polar coordinates. One coordinate is the arc length s along the centreline of the jet. In any cross section of the jet, plane polar coordinates are then taken. In Cartesian coordinates (x, y, z), the centreline of the jet is given by $x = X,\ y = Y$ and $z = Z$ where X, Y and Z are functions of the arc length s and possibly also time t. These are unknown functions which were found in [19] by solving equations that are coupled together with the equations of motion of the fluid. In [19], since the centre line lies in a plane, Y is identically equal to zero. In this current paper, we do not have this condition, and so we have one extra unknown function to find. However, it will become clear during the course of our analysis that we have the same number of equations available to us here as in [19]. We find that we are able to extract a solvability condition from the equations of motion which gives us the extra equation required for closure.

2. Mathematical model

A liquid jet leaves an orifice O on the curved face of a circular cylindrical container of radius s_0. The orifice is itself taken to be circular with radius a. The container rotates about its axis at a constant rate Ω in an anti-clockwise direction when viewed from above relative to fixed axes (x', y', z'). We define a coordinate system (x, y, z) which rotates with the container, having an origin P on the axis of the container, with the orifice positioned at $(s_0, 0, 0)$, see Figure 1. The acceleration due to gravity g acts in the direction of the negative y axis.

We define an orthogonal coordinate system to describe this curved jet. One coordinate will be the arc length s along the centre line of the jet. In any cross section of the jet we also have plane polar coordinates in the radial and azimuthal directions (n, ϕ). These coordinates have unit vectors denoted by $\mathbf{e_s}$, $\mathbf{e_n}$ and $\mathbf{e}_\phi$ respectively, and are shown in Figures 2 and 3. The

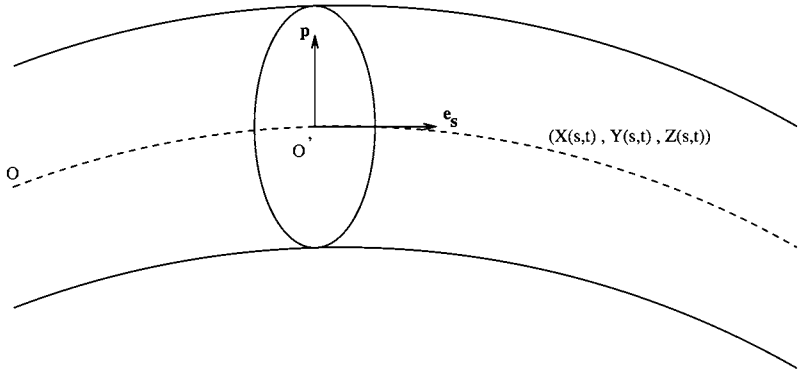

Figure 2. Sketch of the coordinate system, showing the free surface of the jet as bold lines and the centre line of the jet as a dotted line.

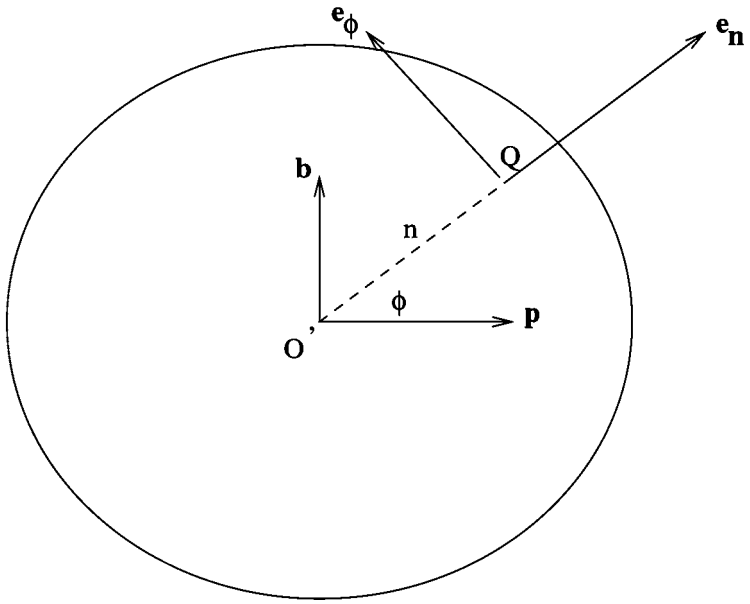

Figure 3. Cross section of the curved jet, showing the radial and azimuthal unit vectors.

centreline of the jet is given by $(X(s,t),\ Y(s,t),\ Z(s,t))$ in the xyz-coordinate system, where X, Y and Z are (as yet) unknown functions of arc length s and time t.

It will be convenient to write some of our expressions and equations in summation notation. In that case, the centreline is written as $\mathbf{r_{cl}} = X_i\ \mathbf{e_i}$, where $\mathbf{e_1} = \mathbf{i}$, $\mathbf{e_2} = \mathbf{j}$, $\mathbf{e_3} = \mathbf{k}$ ($\mathbf{i}$, $\mathbf{j}$ and $\mathbf{k}$ are unit vectors in the xyz-coordinate system and $X_1 = X$, $X_2 = Y$, $X_3 = Z$), and $X_{i,s}^2 = 1$ is the standard arc length condition $X_{1,s}^2 + X_{2,s}^2 + X_{3,s}^2 = 1$ (from $\mathrm{d}s^2 = \mathrm{d}X_1^2 + \mathrm{d}X_2^2 + \mathrm{d}X_3^2$). We calculate the unit vectors in this coordinate system using a principal normal vector $\mathbf{p}$ and a binormal vector $\mathbf{b}$ to the centreline (shown in Figure 3. Using summation notation we write the vectors $\mathbf{e_s}$, $\mathbf{p} = \mathbf{e}_{\mathbf{s}s}/|\mathbf{e}_{\mathbf{s}s}|$ (where $\mathbf{e}_{\mathbf{s}s}$ is the derivative of $\mathbf{e_s}$ with respect to s) and $\mathbf{b} = \mathbf{p} \times \mathbf{e_s}$ as $\mathbf{e_s} = X_{i,s}\mathbf{e_i}$, $\mathbf{p} = X_{i,ss}\mathbf{e_i}/\sqrt{X_{j,ss}X_{j,ss}}$ and $\mathbf{b} = \varepsilon_{ijk}X_{j,ss}X_{k,s}\mathbf{e_i}/\sqrt{X_{L,ss}X_{L,ss}}$ where $\varepsilon_{ijk} = 1$ when $ijk = 123$, 231 or 312, $\varepsilon_{ijk} = -1$ when $ijk = 132$, 321 or 213, and $\varepsilon_{ijk} = 0$ otherwise. Therefore

$$\mathbf{e_n} = \frac{1}{\sqrt{X_{L,ss}X_{L,ss}}}\left(\cos\phi\ X_{i,ss} + \sin\phi\ \varepsilon_{ijk}X_{j,ss}X_{k,s}\right)\ \mathbf{e_i} \tag{1}$$

and

$$\mathbf{e}_\phi = \frac{1}{\sqrt{X_{L,ss}X_{L,ss}}}\left(-\sin\phi X_{i,ss} + \cos\phi\ \varepsilon_{ijk}X_{j,ss}X_{k,s}\right)\ \mathbf{e_i}. \tag{2}$$

Note that the unit vectors are orthogonal to each other (*e.g.* $\mathbf{e_s}\cdot\mathbf{e_n} = 0$ because $X_{i,s}X_{i,ss} = 0$ from the standard arc length condition) and form a right-handed set. The position vector of any particle Q relative to the centre of the orifice O is

$$\mathbf{OQ} = \int_0^s \mathbf{e_s}\,\mathrm{d}s + n\mathbf{e_n}. \tag{3}$$

The structure functions of this coordinate system h_s, h_n and h_ϕ are defined as $h_i = \left|\partial\hat{\mathbf{r}}/\partial i\right|$ for $i = s, n, \phi$, and are found to be $h_n = 1$, $h_\phi = n$ and

$$h_s = \left|\left[X_{i,s} + n\frac{\partial}{\partial s}\left(\frac{\cos\phi X_{i,ss} + \sin\phi\ \varepsilon_{ijk}X_{j,ss}X_{k,s}}{\sqrt{X_{L,ss}X_{L,ss}}}\right)\right]\mathbf{e_i}\right|. \tag{4}$$

The flow is described by the velocity vector $\mathbf{u} = u\mathbf{e_s} + v\mathbf{e_n} + w\mathbf{e}_\phi$ and pressure p (for a liquid with constant density ρ). The free surface is positioned at $n = R\,(s, \phi, t)$. We non-dimensionalise using the following transformations

$$\begin{aligned}
&\bar{u} = \frac{u}{U}, \quad \bar{v} = \frac{v}{U}, \quad \bar{w} = \frac{w}{U}, \quad \bar{p} = \frac{p}{\rho U^2}, \quad \bar{n} = \frac{n}{a}, \quad \varepsilon = \frac{a}{s_0},\\
&\bar{R} = \frac{R}{a}, \quad \bar{s} = \frac{s}{s_0}, \quad \bar{t} = \frac{tU}{s_0}, \quad \bar{X} = \frac{X}{s_0}, \quad \bar{Y} = \frac{Y}{s_0}, \quad \bar{Z} = \frac{Z}{s_0},
\end{aligned} \tag{5}$$

where U is the speed of the jet (in the rotating coordinate system) on leaving the orifice. Using these scalings and dropping overbars for convenience we obtain the continuity equation $\nabla\cdot\mathbf{u} = 0$ as

$$\varepsilon n\frac{\partial u}{\partial s} + \bar{h}_s v + nv\frac{\partial \bar{h}_s}{\partial n} + n\bar{h}_s\frac{\partial v}{\partial n} + w\frac{\partial \bar{h}_s}{\partial \phi} + \bar{h}_s\frac{\partial w}{\partial \phi} = 0, \tag{6}$$

where

$$\bar{h}_s = \left|\left[X_{i,s} + \varepsilon n\frac{\partial}{\partial s}\left(\frac{\cos\phi X_{i,ss} + \sin\phi\ \varepsilon_{ijk}X_{j,ss}X_{k,s}}{\sqrt{X_{L,ss}X_{L,ss}}}\right)\right]\mathbf{e_i}\right|. \tag{7}$$

In dimensional variables, Euler's equations are given by

$$\frac{\partial \mathbf{u}}{\partial t} + (\mathbf{u}.\nabla)\mathbf{u} = -\frac{1}{\rho}\nabla p + \mathbf{g} - 2\boldsymbol{\omega} \times \mathbf{u} - \boldsymbol{\omega} \times (\boldsymbol{\omega} \times \mathbf{r}). \tag{8}$$

Using the identities $(\mathbf{u}\cdot\nabla)\mathbf{u} = \nabla\left(\frac{1}{2}\mathbf{u}^2\right) - \mathbf{u}\times\nabla \times \mathbf{u}$ and $\nabla^2\mathbf{u} = \nabla(\nabla\cdot\mathbf{u}) - \nabla \times (\nabla \times \mathbf{u})$, we can write these in invariant form. Using the fact that $\mathbf{g} = -g\,\mathbf{j}$ and $-2\boldsymbol{\omega} \times \mathbf{u} - \boldsymbol{\omega} \times (\boldsymbol{\omega} \times \mathbf{r}) = (-2\Omega w + \Omega^2 x)\mathbf{i} + (2\Omega u + \Omega^2 z)\mathbf{k}$, where $\omega = (0, \Omega, 0)$, $\mathbf{r} = (x, y, z)$, shifting the origin to the orifice O (so that $X = Y = Z = 0$ at the orifice at $s = 0$), and by taking into account the temporal rate of change of unit vectors $\mathbf{e_n}$, $\mathbf{e_n}$ and $\mathbf{e}_\phi$ in this system, we obtain non-dimensionalized Euler's equations as

$$\varepsilon\frac{\partial u}{\partial t} + \bar{T}_s + \varepsilon\frac{u}{\bar{h}_s}\frac{\partial u}{\partial s} + v\frac{\partial u}{\partial n} + \frac{w}{n}\frac{\partial u}{\partial \phi} + \frac{uv}{\bar{h}_s}\frac{\partial \bar{h}_s}{\partial n} + \frac{uw}{n\bar{h}_s}\frac{\partial \bar{h}_s}{\partial \phi} =$$

$$-\frac{\varepsilon}{\bar{h}_s}\frac{\partial p}{\partial s} + \frac{\varepsilon}{F^2}\bar{G}_s + \bar{R}_s, \tag{9}$$

$$\varepsilon\frac{\partial v}{\partial t} + \bar{T}_n + \varepsilon\frac{u}{\bar{h}_s}\frac{\partial v}{\partial s} + v\frac{\partial v}{\partial n} + \frac{w}{n}\frac{\partial v}{\partial \phi} - \frac{u^2}{\bar{h}_s}\frac{\partial \bar{h}_s}{\partial n} - \frac{w^2}{n} =$$

$$-\frac{\partial p}{\partial n} + \frac{\varepsilon}{F^2}\bar{G}_n + \bar{R}_n \tag{10}$$

and

$$\varepsilon\frac{\partial w}{\partial t} + \bar{T}_\phi + \varepsilon\frac{u}{\bar{h}_s}\frac{\partial w}{\partial s} + v\frac{\partial w}{\partial n} + \frac{w}{n}\frac{\partial w}{\partial \phi} - \frac{u^2}{n\bar{h}_s}\frac{\partial \bar{h}_s}{\partial \phi} + \frac{vw}{n} =$$

$$-\frac{1}{n}\frac{\partial p}{\partial \phi} + \frac{\varepsilon}{F^2}\bar{G}_\phi + \bar{R}_\phi, \tag{11}$$

where $\bar{G}_s = -Y_s$,

$$\bar{G}_n = -\frac{Z_s\chi_3}{(\cos\phi\,\chi_4 - X_{ss}\sin\phi)}$$

$$+\frac{(\cos\phi\,(X_{ss}Z_s - Z_{ss}X_s) + Y_{ss}\sin\phi)\,(\sin\phi\,\chi_4 + X_{ss}\cos\phi)}{(\cos\phi\,\chi_4 - X_{ss}\sin\phi)\,\chi_3}, \tag{12}$$

$$\bar{G}_\phi = \frac{1}{\chi_3}\left(\cos\phi\,(X_{ss}Z_s - Z_{ss}X_s) + Y_{ss}\sin\phi\right), \tag{13}$$

$$\bar{R}_s = \frac{\varepsilon}{Rb^2}\left((X+1)\,X_s + ZZ_s\right), \tag{14}$$

$$\bar{R}_n = \frac{1}{\chi_3}\left(-2\varepsilon u Z_s/Rb + \varepsilon\left(X+1\right)/Rb^2\right)\left(\sin\phi\chi_4 + \cos\phi X_{ss}\right)$$
$$+ \frac{\chi_1\left(\chi_2\left(\sin\phi\chi_4 + X_{ss}\cos\phi\right)\right)}{\left(\cos\phi\chi_4 - X_{ss}\sin\phi\right)\chi_3}, \tag{15}$$

$$\bar{R}_\phi = \frac{\left(-2\varepsilon u Z_s/Rb + \varepsilon\left(X+1\right)/Rb^2\right)\left(\cos\phi\chi_4 - \sin\phi X_{ss}\right)}{\chi_3} + \frac{\chi_1\chi_2}{\chi_3}, \tag{16}$$

$$\bar{T}_s = \frac{\varepsilon}{\chi_3}\left(\left(v\cos\phi - w\sin\phi\right)\left(X_s X_{sst} + Y_s Y_{sst} + Z_s Z_{sst}\right)\right.$$
$$+\left(v\sin\phi + w\cos\phi\right)\left(X_s\left(Y_{ss}Z_{st} - Y_{st}Z_{ss}\right)\right.$$
$$\left.\left.+Y_s\left(X_{st}Z_{ss} - X_{ss}Z_{st}\right) + Z_s\left(X_{ss}Y_{st} - X_{st}Y_{ss}\right)\right)\right), \tag{17}$$

$$\bar{T}_n = \left(\frac{\varepsilon u}{\chi_3\left(\cos\phi\left(Y_{ss}Z_s - Z_{ss}Y_s\right) - X_{ss}\sin\phi\right)}\right)$$
$$\times\left[X_{st}\left(\sin\phi\chi_4 + X_{ss}\cos\phi\right)\left(\cos\phi\chi_4 - X_{ss}\sin\phi\right)\right.$$
$$-Y_{st}\left(\cos\phi\left(X_{ss}Z_s - Z_{ss}X_s\right) + Y_{ss}\sin\phi\right)\left(\sin\phi\chi_4 + X_{ss}\cos\phi\right)$$
$$+Z_{st}\left(\cos\phi\left(X_{ss}Y_s - Y_{ss}X_s\right) - Z_{ss}\sin\phi\right)\left(\sin\phi\chi_4 + X_{ss}\cos\phi\right)$$
$$\left.+\left(Y_{st}Z_s - Z_{st}Y_s\right)\chi_3^2\right], \tag{18}$$

$$\bar{T}_\phi = \frac{\varepsilon u}{\chi_3}\left(-\sin\phi\left(X_s X_{sst} + Y_s Y_{sst} + Z_s Z_{sst}\right)\right.$$
$$\times\cos\phi\left(X_s\left(Y_{st}Z_{ss} - Z_{st}Y_{ss}\right)\right.$$
$$\left.\left.+Y_s\left(Z_{st}X_{ss} - X_{st}Z_{ss}\right) + Z_s\left(X_{st}Y_{ss} - Y_{st}X_{ss}\right)\right)\right), \tag{19}$$

$\chi_1 = 2\varepsilon u X_s/Rb + \varepsilon Z/Rb^2$, $\chi_2 = \cos\phi\left(Y_s X_{ss} - Y_{ss}X_s\right) - Z_{ss}\sin\phi$, $\chi_3 = \left(X_{ss}^2 + Y_{ss}^2 + Z_{ss}^2\right)^{\frac{1}{2}}$ and $\chi_4 = Y_{ss}Z_s - Y_s Z_{ss}$.

The kinematic condition is

$$\varepsilon\frac{\partial R}{\partial t} - \varepsilon\frac{\partial n}{\partial t} + \varepsilon\frac{u}{\bar{h}_s}\frac{\partial R}{\partial s} + \frac{w}{n}\frac{\partial R}{\partial\phi} = v \quad \text{on} \quad n = R. \tag{20}$$

The normal stress boundary condition in this inviscid flow is conveniently written as $p = \kappa_1/We$ on $n = R$, where the curvature κ_1 is given by

$$\kappa_1 = \frac{1}{n\bar{h}_s}\left(\varepsilon^2\frac{\partial}{\partial s}\left(\frac{-\frac{n}{h_s}\frac{\partial R}{\partial s}}{E}\right) + \frac{\partial}{\partial n}\left(\frac{nh_s}{E}\right) + \frac{\partial}{\partial\phi}\left(\frac{-\frac{h_s}{n}\frac{\partial R}{\partial\phi}}{E}\right)\right), \tag{21}$$

and

$$E = \left(1 + \frac{\varepsilon^2}{\bar{h}_s^2}\left(\frac{\partial R}{\partial s}\right)^2 + \frac{1}{n^2}\left(\frac{\partial R}{\partial \phi}\right)^2\right)^{\frac{1}{2}}. \tag{22}$$

Also, the arc length condition is $X_s^2 + Y_s^2 + Z_s^2 = 1$, and the no flux boundary conditions on the centreline are $v = w = 0$ on $n = 0$. Conditions at the orifice are given by $X = Y = Y_s = Z = Z_s = 0$, $X_s = 1$, $R = 1 = u = 1$ at $s = 0$. In the above equations (including Euler's equations) we obtain several non-dimensional parameters, the Froude number $F = U/(s_0 g)^{1/2}$, the Rossby number $\mathrm{Rb} = U/(\Omega s_0)$ and the Weber number $\mathrm{We} = \rho U^2 a/\sigma$ (where σ is the surface tension coefficient), describing the relative importance of the forces due to gravity, rotation and surface tension, respectively, as well as the aspect ratio $\varepsilon = a/s_0$.

3. Steady state

We now determine steady solutions to these equations, including the steady trajectory of the jet. We will find that the trajectory of the jet is not the same trajectory as would be taken by a Newtonian particle released from the orifice because of the pressure gradients in the liquid. In order to determine the trajectory we use our coordinate system described in the previous section. We note that we are in an unusual mathematical position: the location of one of the axes of the coordinate system, the jet's centreline (or trajectory), is itself an unknown to be determined in this problem, and we determine the location of this coordinate axis by solving equations that are coupled together with the equations of motion of the liquid (Euler's equations, etc.). Using a slender jet assumption, we seek an expression for the steady state. We pose the expansions

$$u = u_0(s) + \varepsilon u_1(s, n, \phi) + \cdots, \tag{23}$$

$$v = \varepsilon v_1(s, n, \phi) + \varepsilon^2 v_2(s, n, \phi) + \cdots, \tag{24}$$

$$p = p_0(s, n, \phi) + \varepsilon p_1(s, n, \phi) + \cdots, \tag{25}$$

$$R = R_0(s) + \varepsilon R_1(s, \phi) + \cdots, \tag{26}$$

$$X = X_0(s) + \varepsilon X_1(s) + \cdots, \tag{27}$$

$$Y = Y_0(s) + \varepsilon Y_1(s) + \cdots, \tag{28}$$

$$Z = Z_0(s) + \varepsilon Z_1(s) + \cdots, \tag{29}$$

with $w = 0$, so that the velocity at leading-order is tangential to the centreline of the jet. (There may also be solutions for which $w \neq 0$. However, we will leave this additional complexity for future work.) Substituting these expressions in the non-dimensional jet equations (note that we write X_0, Y_0 and Z_0 as X, Y and Z, respectively, for simplicity) we obtain at leading order

$$n u_{0s} + v_1 + n v_{1n} = 0, \tag{30}$$

$$u_0 u_{0s} = -p_{0s} - \frac{Y_s}{F^2} + \frac{1}{\mathrm{Rb}^2}\left((X + 1) X_s + Z Z_s\right), \tag{31}$$

$$p_{0_n} = 0, \tag{32}$$

$$u_0^2 \cos\phi \left(X_{ss}^2 + Y_{ss}^2 + Z_{ss}^2\right)^{\frac{1}{2}} = -p_{1n}$$

$$-\frac{1}{F^2}\frac{Z_s \left(X_{ss}^2 + Y_{ss}^2 + Z_{ss}^2\right)^{\frac{1}{2}}}{\left(\cos\phi \left(Y_{ss}Z_s - Y_s Z_{ss}\right) - X_{ss}\sin\phi\right)}$$

$$+\frac{\left(\sin\phi \left(Y_{ss}Z_s - Z_{ss}Y_s\right) + X_{ss}\cos\phi\right)\left(\cos\phi \left(X_{ss}Z_s - X_s Z_{ss}\right) + Y_{ss}\sin\phi\right)}{F^2 \left(\cos\phi \left(Y_{ss}Z_s - Y_s Z_{ss}\right) - X_{ss}\sin\phi\right)\left(X_{ss}^2 + Y_{ss}^2 + Z_{ss}^2\right)^{\frac{1}{2}}}$$

$$+\left(-\frac{2u_0 Z_s}{\mathrm{Rb}} + \frac{X+1}{\mathrm{Rb}^2}\right)\left(\frac{\sin\phi \left(Y_{ss}Z_s - Z_{ss}Y_s\right) + X_{ss}\cos\phi}{\left(X_{ss}^2 + Y_{ss}^2 + Z_{ss}^2\right)^{\frac{1}{2}}}\right)$$

$$-\left(\frac{2u_0 X_s}{\mathrm{Rb}} + \frac{Z}{\mathrm{Rb}^2}\right)\left(\frac{Y_s \left(X_{ss}^2 + Y_{ss}^2 + Z_{ss}^2\right)^{\frac{1}{2}}}{\left(\cos\phi \left(Y_{ss}Z_s - Z_{ss}Y_s\right) - X_{ss}\sin\phi\right)} - Q\right), \tag{33}$$

$$p_{0_\phi} = 0, \tag{34}$$

$$-u_0^2 \sin\phi \left(X_{ss}^2 + Y_{ss}^2 + Z_{ss}^2\right)^{\frac{1}{2}} = -\frac{1}{n}p_{1\phi}$$

$$+\frac{1}{F^2}\frac{\left(\cos\phi \left(X_{ss}Z_s - X_s Z_{ss}\right) + Y_{ss}\sin\phi\right)}{\left(X_{ss}^2 + Y_{ss}^2 + Z_{ss}^2\right)^{\frac{1}{2}}}$$

$$+\left(-\frac{2u_0 Z_s}{\mathrm{Rb}} + \frac{X+1}{\mathrm{Rb}^2}\right)\left(\frac{\cos\phi \left(Y_{ss}Z_s - Z_{ss}Y_s\right) - X_{ss}\sin\phi}{\left(X_{ss}^2 + Y_{ss}^2 + Z_{ss}^2\right)^{\frac{1}{2}}}\right)$$

$$+\left(\frac{2u_0 X_s}{\mathrm{Rb}} + \frac{Z}{\mathrm{Rb}^2}\right)\left(\frac{\left(\cos\phi \left(Y_s X_{ss} - Y_{ss}X_s\right) - Z_{ss}\sin\phi\right)}{\left(X_{ss}^2 + Y_{ss}^2 + Z_{ss}^2\right)^{\frac{1}{2}}}\right), \tag{35}$$

$u_0 R_{0_s} = v_1$ on $n = R_0$, $p_0 = 1/n\mathrm{We}$ on $n = R_0$,

$$p_1 = -\frac{1}{\mathrm{We}}\left(-\frac{1}{R_0^2}\left(R_1 + R_{1\phi\phi}\right) + \cos\phi \left(X_{ss}^2 + Y_{ss}^2 + Z_{ss}^2\right)^{\frac{1}{2}}\right)$$

on $n = R_0$, (36)

$v_1 = 0$ on $n = 0$, and $X_s^2 + Y_s^2 + Z_s^2 = 1$, where $Q = Q_1 Q_2 / (Q_3 Q_4)$ and $Q_1 = \cos\phi \left(Y_s X_{ss} - Y_{ss}X_s\right) - Z_{ss}\sin\phi$, $Q_2 = \sin\phi \left(Y_{ss}Z_s - Y_s Z_{ss}\right) + X_{ss}\cos\phi$, $Q_3 = \cos\phi \left(Y_{ss}Z_s - Z_{ss}Y_s\right) - X_{ss}\sin\phi$, and $Q_4 = \left(X_{ss}^2 + Y_{ss}^2 + Z_{ss}^2\right)^{\frac{1}{2}}$.

Solving this set of equations we obtain

$$p_0 = \frac{1}{R_0 \mathrm{We}}, \tag{37}$$

$$u_0 = \left(1 - \frac{2Y}{F^2} + \frac{1}{\mathrm{Rb}^2}\left(X^2 + 2X + Z^2\right) + \frac{2}{\mathrm{We}}\left(1 - \frac{1}{R_0}\right)\right)^{\frac{1}{2}}, \tag{38}$$

$$v_1 = -\frac{n}{2}\frac{\mathrm{d}u_0}{\mathrm{d}s}, \tag{39}$$

$$p_1 = -\frac{n}{\mathrm{We}R_0}\cos\phi\left(X_{ss}^2 + Y_{ss}^2 + Z_{ss}^2\right)^{\frac{1}{2}} - h_1(s), \tag{40}$$

$$\frac{Z_s X_{ss} - X_s Z_{ss}}{F^2} - \frac{2Y_{ss}u_0}{\mathrm{Rb}} + \frac{(X+1)\left(Y_{ss}Z_s - Z_{ss}Y_s\right)}{\mathrm{Rb}^2} + \frac{Z\left(Y_s X_{ss} - Y_{ss}X_s\right)}{\mathrm{Rb}^2} = 0, \tag{41}$$

$$\left(u_0^2 - \frac{1}{\mathrm{We}R_0}\right)\left(X_{ss}^2 + Y_{ss}^2 + Z_{ss}^2\right) = -\frac{Y_{ss}}{F^2} + \frac{2u_0}{\mathrm{Rb}}\left(X_s Z_{ss} - Z_s X_{ss}\right) + \frac{1}{\mathrm{Rb}^2}\left((X+1)X_{ss} + ZZ_{ss}\right) \tag{42}$$

$$\text{and} \quad \frac{\mathrm{d}R_0}{\mathrm{d}s} = \frac{R_0\left(Y_s/F^2 - \left((X+1)X_s + ZZ_s\right)/\mathrm{Rb}^2\right)}{2\left(u_0^2 + 1/(2WeR_0)\right)}, \tag{43}$$

where $h_1(s)$ could be found at next order.

We note that Equation (41) is a solvability condition. As discussed in the introduction, comparing this trajectory calculation to the one carried out in [19], we have one extra unknown function here (namely Y). This is because the centreline here does not lie in a plane due to the action of gravity. Equation (41) is the extra equation needed for us to close our system. Note that as $F \to \infty$ with $Y = 0$, the above set of equations tends to those in [19], and Equation (41) becomes identically satisfied. Equation (41) arises as follows. Equations (33) and (35) can be manipulated to give

$$\sin\phi\frac{\partial p_1}{\partial n} + \frac{\cos\phi}{n}\frac{\partial p_1}{\partial \phi} = H(s), \tag{44}$$

where $H(s)$ is a function of s only. Therefore, $p_1 = n\sin\phi H(s) + n\cos\phi g(s) - h_1(s)$, where $g(s)$ is some function of s only. Boundary condition (36) then gives a second-order ordinary differential equation for R_1. Since R_1 must be periodic with period 2π, it must not have particular solutions of the form $\phi\cos\phi$ or $\phi\sin\phi$. Therefore the inhomogeneous parts of this differential equation which could drive such non-periodic terms must have zero coefficients. Therefore, $H(s) = 0$ which gives Equation (41), as well as an equation for $g(s)$.

We solve these equations numerically (using a Runge-Kutta-Merson scheme - NAG library routine D02BBF) subject to the initial conditions $X_s = 1$, $X = Y = Y_s = Z = Z_s = 0$ and $R_0 = u_0 = 1$. Figure 4 shows the centrelines of jets for various Weber numbers. We see that the centreline forms a helical shape with growing radius as it leaves the orifice. Making the Weber number smaller has the effect of making the loops coil more tightly and fall more sharply.

Figure 5 shows the centre lines of jets for different Froude numbers. Decreasing the Froude number has the effect of making the jet fall faster. Figure 6 shows the centrelines of jets for different Rossby numbers. Decreasing the Rossby number makes the jet coil more tightly.

Examining the small s asymptotics of our steady equations we find

$$X = s - \frac{\mathrm{We}^2\left(\mathrm{Rb}^2 + 4F^4\right)}{6F^4\mathrm{Rb}^2(1-\mathrm{We})^2}s^3 + O(s^4)\ , \tag{45}$$

$$Y = \frac{\mathrm{We}}{2F^2(1-\mathrm{We})}s^2 + O(s^3)\ , \tag{46}$$

$$Z = \frac{\mathrm{We}}{\mathrm{Rb}(\mathrm{We}-1)}s^2 + O(s^3)\ , \tag{47}$$

$$R_0 = 1 - \frac{\mathrm{We}}{\mathrm{Rb}^2(2\mathrm{We}+1)}s + O(s^2) \tag{48}$$

and

$$u_0 = 1 + \frac{2\mathrm{We}}{\mathrm{Rb}^2(2\mathrm{We}+1)}s + O(s^2)\ . \tag{49}$$

Note there is 0 singularity at $\mathrm{We} = 1$, which we also find in numerical solutions. This singularity has also been found in other problems [17, 20–22], and our numerical solutions close to $\mathrm{We} = 1$ have features in common with the ones found in these papers [23, pp. 65–72]. This singularity can be removed by imposing more specific exit conditions for the jet at the nozzle (as described in [21–22]), and arises because the jet is significantly affected by the menisci at the contact point with the solid surface when the Weber number is small. However, in prilling, the Weber number is large and the results presented here are unaffected by this singularity, and so this is not of immediate concern in this paper. This is the subject of ongoing research.

4. Temporal stability

We now perturb about the steady state found in the previous section to analyse the temporal stability of our solution. We perturb the velocity field by adding onto $\mathbf{u}$ a time-dependent perturbation $\delta\tilde{\mathbf{u}}$, where δ is small. We perturb the pressure p by adding on a time-dependent perturbation $\delta\tilde{p}$. We perturb the position of the free surface R by adding on $\delta\tilde{R}$. We perturb X, Y and Z by adding on $\delta\varepsilon\tilde{X}$, $\delta\varepsilon\tilde{Y}$ and $\delta\varepsilon\tilde{Z}$. (Note that if the ε's in the perturbation for the position of the centreline are omitted then it is possible to show that the leading-order perturbations for X, Y and Z in ε are identically equal to zero, and the first non-zero pertubations

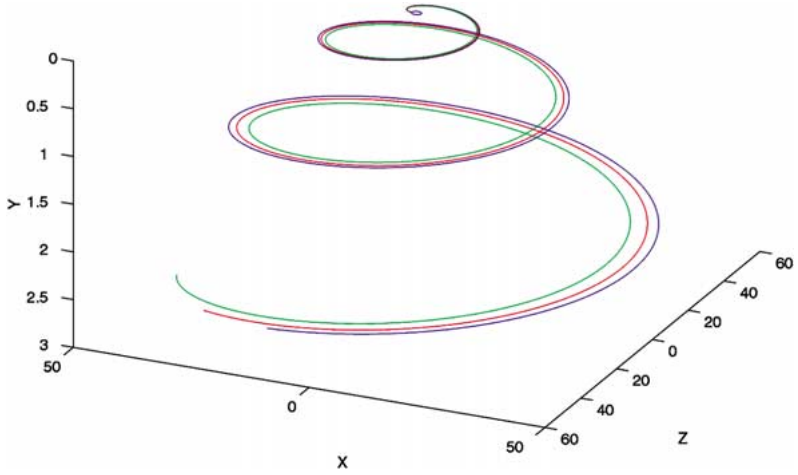

Figure 4. Graph of the centre line of various jets for $F = 16$ and Rb $= 2$. The lines show We $= 50$, We $= 18000$ and We $= 20$. The tightest coiled curve corresponds to the smallest Weber number and the least tightly coiled curve has the largest Weber number. The small circle next to the start of the jet shows the container.

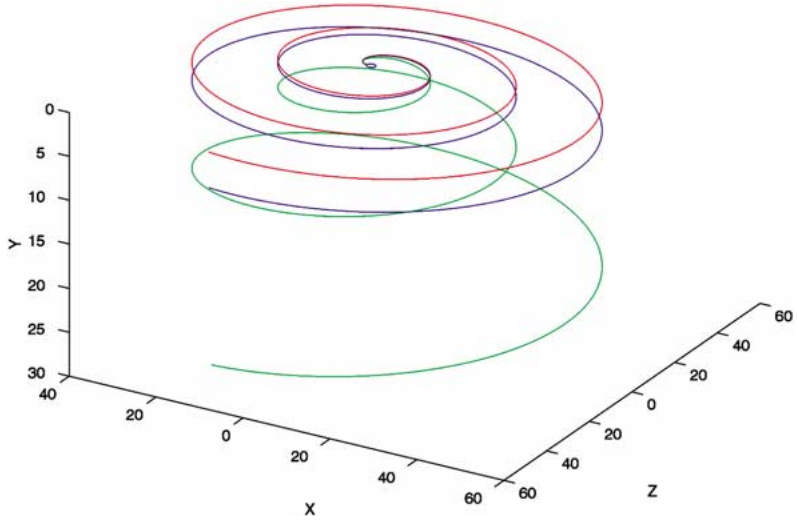

Figure 5. Graph of the centre line of various jets for Rb $= 2$ and We $= \infty$. The lines show $F = 16$, $F = 10$ and $F = 5$. The curve which falls most rapidly is for the smallest Froude number. The curve which falls the least is for the largest Froude number. The circle shows the container.

are those given here.) Since droplets produced by jet instability have a radius comparable to the radius of the jet we must introduce a multiple length scale into our stability analysis [19]. Looking for a distinguished limit we find that all of these perturbations are functions of $s, \bar{s}, t$ and $\bar{t}$ where $\bar{s} = s/\varepsilon$ and $\bar{t} = t/\varepsilon$. Perturbations of the velocity and the pressure ($\tilde{\mathbf{u}}$ and $\tilde{p}$) are additionally functions of n and ϕ, while the perturbation for the free surface $\tilde{R}$ is a function of ϕ in addition to $s, \bar{s}, t$ and $\bar{t}$.

We substitute the above perturbations in our equations and find the $O(\delta)$ equations. At leading order in ε these give

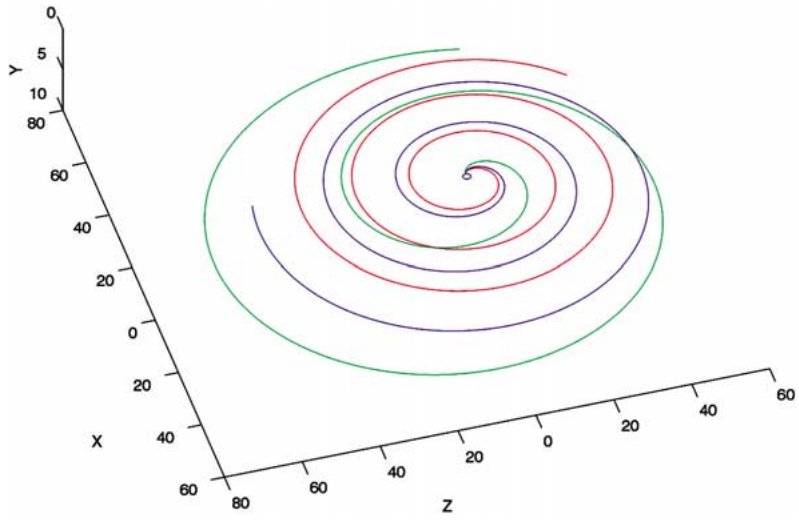

Figure 6. Graph of the centre line of various jets for $F = 16$ and $\mathrm{We} = \infty$. The lines show $\mathrm{Rb} = 1$, $\mathrm{Rb} = 2$ and $\mathrm{Rb} = 5$. The most tightly coiled curve is for the smallest Rossby number. The least tightly coiled curve is for the highest Rossby number. The circle shows the container.

$$n\frac{\partial \tilde{u}}{\partial \bar{s}} + \tilde{v} + n\frac{\partial \tilde{v}}{\partial n} + \frac{\partial \tilde{w}}{\partial \phi} = 0, \tag{50}$$

$$\frac{\partial \tilde{u}}{\partial \bar{t}} + u_0(s)\frac{\partial \tilde{u}}{\partial \bar{s}} = -\frac{\partial \tilde{p}}{\partial \bar{s}}, \tag{51}$$

$$\frac{\partial \tilde{v}}{\partial \bar{t}} + u_0(s)\frac{\partial \tilde{v}}{\partial \bar{s}} - u_0(s)\cos\phi P_1 - \cos\phi\, u_0^2(s) P_2 = -\frac{\partial \tilde{p}}{\partial n}, \tag{52}$$

$$\frac{\partial \tilde{w}}{\partial \bar{t}} + u_0(s)\frac{\partial \tilde{w}}{\partial \bar{s}} + u_0(s)\sin\phi P_1 + \sin\phi\, u_0^2(s) P_2 = -\frac{1}{n}\frac{\partial \tilde{p}}{\partial \phi}, \tag{53}$$

$$\frac{\partial \tilde{R}}{\partial \bar{t}} + \cos\phi\left(\left(X_{ss}^2 + Y_{ss}^2 + Z_{ss}^2\right)^{-\frac{1}{2}}\left(X_{ss}\frac{\partial \tilde{X}}{\partial \bar{t}} + Y_{ss}\frac{\partial \tilde{Y}}{\partial \bar{t}} + Z_{ss}\frac{\partial \tilde{Z}}{\partial \bar{t}}\right)\right)$$

$$-\tilde{v} + u_0(s)\frac{\partial \tilde{R}}{\partial \bar{s}} = 0 \quad \text{on} \quad n = R_0, \tag{54}$$

$$\tilde{p} = \frac{1}{\mathrm{We}}\left(-\frac{1}{R_0^2}\left(\tilde{R} + \frac{\partial^2 \tilde{R}}{\partial \phi^2}\right) + \cos\phi P_2 - \frac{\partial^2 \tilde{R}}{\partial \bar{s}^2}\right) \quad \text{on} \quad n = R_0, \tag{55}$$

$$\tilde{v} = \tilde{w} = 0 \quad \text{on} \quad n = 0, \tag{56}$$

$$X_s\frac{\partial \tilde{X}}{\partial \bar{s}} + Y_s\frac{\partial \tilde{Y}}{\partial \bar{s}} + Z_s\frac{\partial \tilde{Z}}{\partial \bar{s}} = 0 \tag{57}$$

and

$$0 = \left(\frac{Z}{\mathrm{Rb}^2} - \frac{2u_0 X_s}{\mathrm{Rb}}\right)\left(Y_s\frac{\partial\tilde{X}}{\partial^2\bar{s}} - X_s\frac{\partial\tilde{Y}}{\partial^2\bar{s}}\right)$$

$$+\frac{1}{F^2}\left(Z_s\frac{\partial\tilde{X}}{\partial^2\bar{s}} - X_s\frac{\partial\tilde{Z}}{\partial^2\bar{s}}\right) + \left(\frac{(X+1)}{\mathrm{Rb}^2} - \frac{2u_0 Z_s}{\mathrm{Rb}}\right)\left(Z_s\frac{\partial\tilde{Y}}{\partial^2\bar{s}} - Y_s\frac{\partial\tilde{Z}}{\partial^2\bar{s}}\right), \tag{58}$$

where

$$P_1 = \left(X_{ss}^2 + Y_{ss}^2 + Z_{ss}^2\right)^{-\frac{1}{2}}\left(X_{ss}\frac{\partial^2\tilde{X}}{\partial\bar{s}\partial\bar{t}} + Y_{ss}\frac{\partial^2\tilde{Y}}{\partial\bar{s}\partial\bar{t}} + Z_{ss}\frac{\partial^2\tilde{Z}}{\partial\bar{s}\partial\bar{t}}\right), \tag{59}$$

$$P_2 = \left(X_{ss}^2 + Y_{ss}^2 + Z_{ss}^2\right)^{-\frac{1}{2}}\left(X_{ss}\frac{\partial^2\tilde{X}}{\partial^2\bar{s}} + Y_{ss}\frac{\partial^2\tilde{Y}}{\partial^2\bar{s}} + Z_{ss}\frac{\partial^2\tilde{Z}}{\partial^2\bar{s}}\right), \tag{60}$$

We solve these equations by posing modal expansions, and also by expanding the ϕ-dependent perturbations into Fourier series in ϕ. Thus

$$\left(\tilde{u}, \tilde{v}, \tilde{w}, \tilde{p}, \tilde{R}\right) = T\left(\left(\mathrm{i}\bar{u}_1(n,s), \bar{v}_1(n,s), \bar{w}_1(n,s), \bar{p}_1(n,s), \bar{R}_1(s)\right)\right.$$
$$+\sum_{m=1}^{\infty}\left(\mathrm{i}\bar{u}_{m0}(n,s), \bar{v}_{m0}(n,s), \bar{w}_{m0}(n,s), \bar{p}_{m0}(n,s), \bar{R}_{m0}(s)\right)\cos(m\phi)$$
$$\left.+\left(\mathrm{i}\bar{u}_{m1}(n,s), \bar{v}_{m1}(n,s), \bar{w}_{m1}(n,s), \bar{p}_{m1}(n,s), \bar{R}_{m1}(s)\right)\sin(m\phi)\right) + \text{c.c}, \tag{61}$$

$\tilde{X} = T\bar{X}_1 + \text{c.c.}$, $\tilde{Y} = T\bar{Y}_1 + \text{c.c.}$ and $\tilde{Z} = T\bar{Z}_1 + \text{c.c.}$, where c.c. denotes complex conjugate, and

$$T = \exp(\mathrm{i}k(s)\bar{s} + \lambda(s)\bar{t}). \tag{62}$$

These equations are then easily solved and we obtain expressions for the eigenvalues $\lambda = \lambda_m$ where

$$\lambda_m = -\mathrm{i}ku_0 \pm \sqrt{\frac{1}{\mathrm{We}}\left(\frac{1}{R_0^2}\left(1-m^2\right) - k^2\right)k\frac{I_m'(kR_0)}{I_m(kR_0)}}, \tag{63}$$

and I_m is a modified Bessel function. For $m > 0$ this gives an infinite set of neutrally stable modes. The axisymmetric mode corresponding to $m = 0$ can be unstable. The perturbations associated with this mode are found to be

$$\bar{u}_1 = A_1(s)I_0(kn), \quad \bar{v}_1 = A_1(s)I_1(kn),$$
$$\bar{w}_1 = 0, \quad \bar{p}_1 = -A_1(s)\frac{\lambda + \mathrm{i}ku_0}{k}I_0(kn),$$
$$\bar{R}_1 = \frac{\bar{v}_1}{\lambda + \mathrm{i}ku_0}, \tag{64}$$

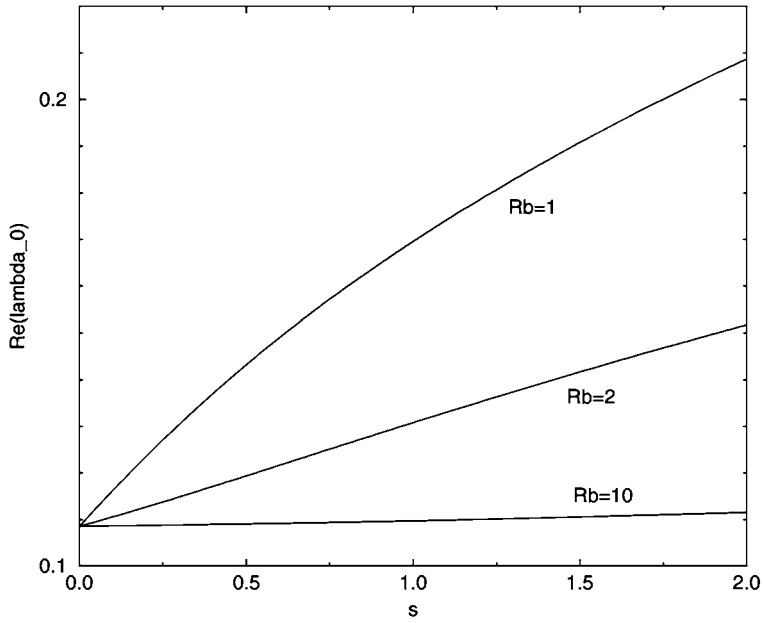

Figure 7. Graph showing the growth rate $\Re\mathfrak{e}(\lambda_0)$ of the most unstable mode against s for various Rossby numbers (We $= 10$, $F = 10$). The top line shows Rb $= 1$, the middle line Rb $= 2$ and the bottom line Rb $= 10$.

where $A_1(s)$ could be determined at the next order. Note that this mode appears to be the same mode as found in [1] for a straight jet. However, here R_0, u_0, k and λ_m are all functions of the arc length s, whereas they are all constant for Rayleigh's straight jet. This mode is unstable when $0 < k < 1/R_0$, and the maximum value of the growth rate $\Re e(\lambda_0)$ occurs when $k = k^* = 0.697/R_0$. (Note that the perturbations associated with the neutrally stable modes are given by lengthy expressions which can be found in [23].)

Figures 7 and 8 show the growth rate of the most unstable mode plotted against arc length for various parameter values. We see that the mode grows more quickly for lower values of Rb or F.

5. Spatial stability and break up length

We now consider a mode of the form $\exp\left(\mathrm{i}k(s)\bar{s} + \lambda(s)\bar{t}\right)$ where k is considered complex, while λ $(= -\mathrm{i}\omega)$ is purely imaginary (and ω is the real frequency). The mode is unstable when $\Im\mathfrak{m}(k) < 0$, and the largest growth rate corresponds to the most negative value of $\Im\mathfrak{m}(k)$. This spatial stability approach is physically more relevant than the temporal stability approach described in the previous section when the jet emerges from a nozzle [3].

Figures 9 and 10 show numerical solutions of the eigenvalue relation for the mode $m = 0$. The figures show $\Re\mathfrak{e}(k)$ and $\Im\mathfrak{m}(k)$ respectively for the most unstable mode for each value of s. The most unstable mode is found by maximising the growth rate $-\Im\mathfrak{m}(k)\bar{s}$ for each value of s.

By varying the parameters we find that increasing the Froude number F (while holding We and Rb fixed) increases the growth rate of the mode $|\bar{s}\Im\mathfrak{m}(k)|$; increasing the Rossby number Rb (while holding We and F fixed) increases the growth rate; increasing the Weber number We (while holding Rb and F fixed) decreases the growth rate. Reference [23] contains many

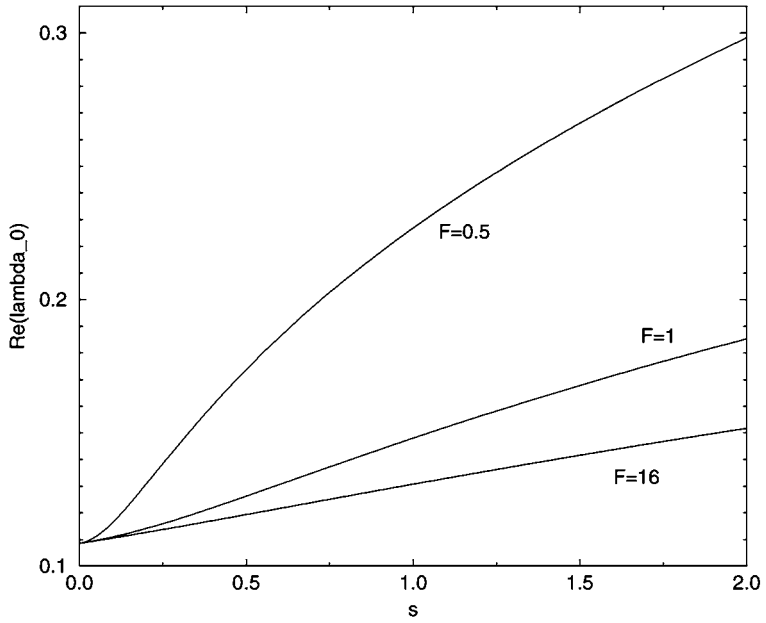

Figure 8. Graph showing the growth rate $\mathfrak{Re}(\lambda_0)$ of the most unstable mode against s for various Froude numbers (Rb $= 2$, We $= 10$). The top line shows $F = 0{\cdot}5$, the middle line $F = 1$ and the bottom line $F = 16$.

graphs from an extensive investigation of the three parameter space (We, F and Rb) for both the steady state and linear stability calculations.

Comparing Figures 7 and 10 we see that decreasing Rb (*i.e.* increasing the rate of rotation) increases the growth rate of a mode growing with time, but decreases the growth rate of a mode growing with distance along the jet. These statements are not contradictory since the speed of the jet (the speed of the steady mean flow and the speed of time-dependent disturbances) increases when Rb is decreased. Similar comments apply to variations with F.

The linear stability results can be used to estimate the break up length of the jet. This is achieved by equating the leading-order steady solution for the free surface and the modulus of the leading-order unsteady solution for the perturbation of the free surface. We can prove that the small parameter δ is equal to $\sqrt{\varepsilon}$ by using a distinguished limit argument on the nonlinear perturbation equations (see [5,19,23]). Figure 11 shows the ratio of the break up length of the jet to the radius of the jet plotted against $\sqrt{\text{We}}$ for three different combinations of the Froude and Rossby numbers. Here we have chosen $|A| = 0{\cdot}01$ and $\varepsilon = 0{\cdot}01$. Note that the lines on this graph are straight. This is the same as for a straight jet [14].

6. Conclusions

We have developed an asymptotic method to enable us to examine free liquid jets arising in prilling. These jets are subjected to rotation, gravity and surface tension. Using a solvability argument we have been able to determine nonlinear ordinary differential equations for the steady trajectory. The linear stability of these steady solutions can be determined. Using multiple scales, we find that the wavelength, wavespeed and growth rate of a linear mode vary with distance along the jet. This analysis enables us to estimate the break up length of the jet. We find that the breakup length of the jet increases with Weber number. Increasing the

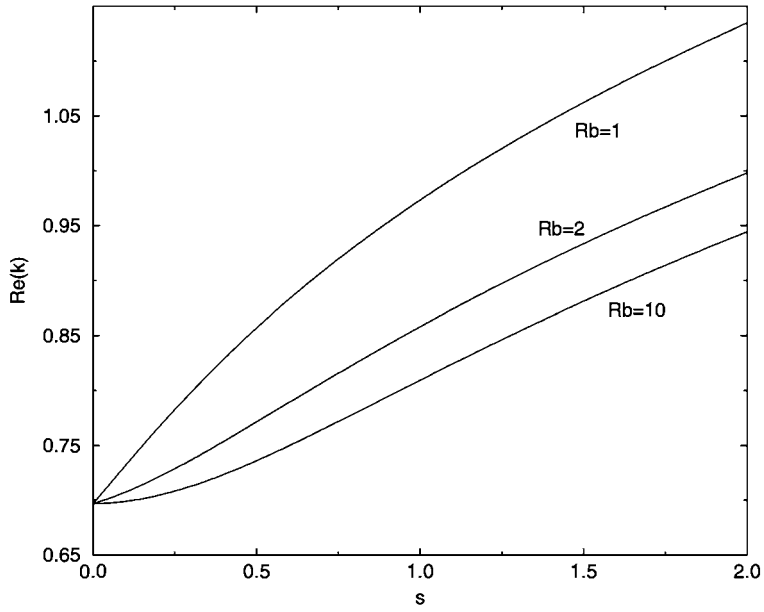

Figure 9. Graph showing $\mathfrak{Re}(k)$ for the most unstable mode against s for various values of the Rossby number (We $= 100$, $F = 1$). The top line shows Rb $= 1$, the middle line Rb $= 2$ and the bottom line Rb $= 10$.

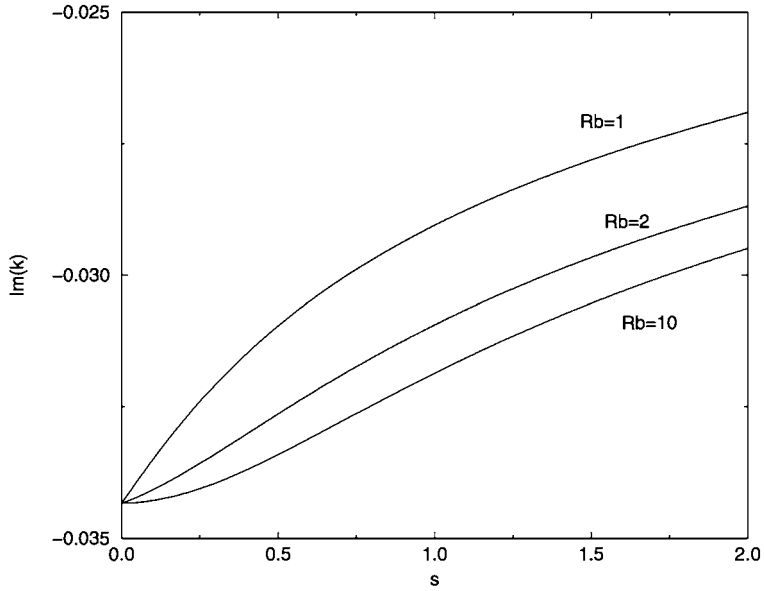

Figure 10. Graph showing $\mathfrak{Im}(k)$ for the most unstable mode against s for various values of the Rossby number ($F = 1$, We $= 100$). The top line shows Rb $= 1$, the middle line Rb $= 2$ and the bottom line Rb $= 10$.

Rossby number or Froude number is found to decrease the break up length of the jet. We note that nonlinear effects will become important during break up and a fully nonlinear unsteady calculation is required to fully understand break up.

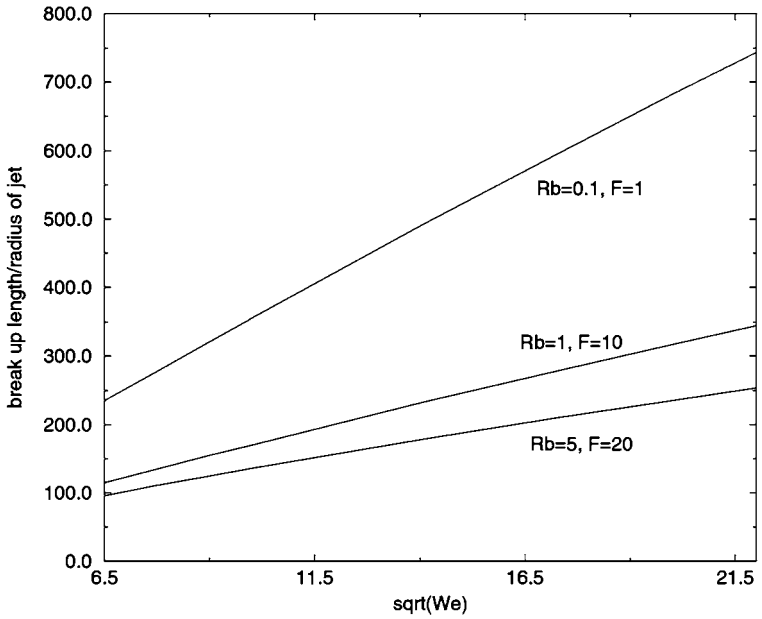

Figure 11. Graph showing an estimate of the break up length of the jet divided by the radius of the jet plotted against $\sqrt{\mathrm{We}}$ for various Froude and Rossby numbers obtained from the linear (spatial) stability analysis. The top line represents Rb $= 0{\cdot}1$, $F = 1$, the middle line Rb $= 1$, $F = 10$ and the bottom line Rb $= 5$, $F = 20$ ($|A| = 0.01$ and $\varepsilon = 0{\cdot}01$).

7. Acknowledgements

The authors thank Dr R.M.S.M. Schulkes for useful discussions of this work. I.M.W. thanks *Norsk Hydro* and EPSRC for their financial support.

References

1. J.W.S. Rayleigh, On the instability of jets. *Proc. London Math. Soc.* 10 (1878) 4–13.
2. C. Weber, Zum Zerfall eines Flüssigkeitsstrahles. *Z. Angew. Math. Mech.* 11 (1931) 136–141.
3. J.B. Keller, S.I. Rubinow and Y.O. Tu, Spatial instability of a jet. *Phys. Fluids* 16 (1973) 2052–55.
4. J. Eggers, Universal pinching of 3D axisymmetric free-surface flow. *Phys. Rev. Letters* 71 (1993) 3458–60.
5. R.M.S.M. Schulkes, Dynamics of liquid jets revisited. *J. Fluid Mech.* 250 (1993) 635–650.
6. D.T. Papageorgiou, Analytical description of the breakup of liquid jets. *J. Fluid Mech.* 301 (1995) 109–132.
7. J.H. Hilbing and S.D. Heister, Droplet size control in liquid jet breakup. *Phys. Fluids* 8, 6 (1996) 1574–81.
8. R.J. Donnelly and W. Glaberson, Experiments on the capillary instability of a liquid jet. *Proc. R. Soc. London* A 290 (1966) 547–556.
9. E.F. Goedde and M.C. Yuen, Experiments on liquid jet instability. *J. Fluid Mech.* 40 (1970) 495–511.
10. K.C. Chaudhary and T. Maxworthy, The nonlinear capillary instability of a liquid jet. Part 2. Experiments on jet behaviour before droplet formation. *J. Fluid Mech.* 96 (1980) 275–286.
11. K.C. Chaudhary and T. Maxworthy, The nonlinear capillary instability of a liquid jet. Part 3. Experiments on satellite drop formation and control. *J. Fluid Mech.* 96 (1980) 287–297.
12. J.N. Anno, *The Mechanics of Liquid Jets.* Lexington, Mass: Lexington Books. (1977) 208 pp.
13. D.B. Bogy, Drop formation in a circular liquid jet. *Annu. Rev. Fluid. Mech.* 11 (1979) 207–228.
14. S. Middleman, *Modeling Axisymmetric flows: Dynamics of Films, Jets, and Drops.* San Diego; London: Academic Press (1995) 267 pp.
15. J. Eggers, Nonlinear dynamics and breakup of free-surface flows. *Rev. Mod. Phy.* 69 (1997) 865–929.
16. J.B. Keller and M.L. Weitz, Upward ‘falling’ jets and surface tension. *J. Fluid Mech.* 2 (1957) 201–203.

17. J.B. Keller and J. Geer, Flows of thin streams with free boundaries. *J. Fluid Mech.* 59 (1973) 417–432.
18. E.O. Tuck, The shape of free jets of water under gravity. *J. Fluid Mech.* 76 (1976) 625–640.
19. I.M. Wallwork, S.P. Decent, A.C. King and R.M.S.M. Schulkes, The trajectory and stability of a spiralling liquid jet: Part I. Inviscid theory. To appear in *J. Fluid Mech.* (2002)
20. M.H.I. Baird and J.F. Davidson, Annular jets - Fluid dynamics. *Chem. Engng. Sci.* 17 (1962) 467–472.
21. D.S. Finnicum, S.J. Weinstein and K.J. Ruschak, The effect of applied pressure on the shape of a two-dimensional liquid curtain falling under the influence of gravity. *J. Fluid Mech.* 255 (1993) 647–665.
22. J.I. Ramos, Upward and Downward annular liquid jets: Conservation properties, singularities, and numerical errors. *Appl. Math. Modelling* 20 (1996) 440–458.
23. I.M. Wallwork, *The Trajectory and Stability of Spiralling Liquid Jets.* Birmingham: PhD thesis. University of Birmingham (2001) 259 pp.